Research Square

Preprints are preliminary reports that have not undergone peer review.
They should not be considered conclusive, used to inform clinical practice,
or referenced by the media as validated information.

A Data-Driven Surrogate Model for Tool Design Optimization in Multi-Stage Shear Cutting and Collar Forming Processes

Daniel Luca Hahn

daniel.luca.hahn@iwu.fraunhofer.de

Fraunhofer Institute for Machine Tools and Forming Technology IWU

Frederik Fonger

University of Bayreuth

Patrik Thomas Michalski

Kiel University

Matthias Riemer

Fraunhofer Institute for Machine Tools and Forming Technology IWU

Verena Kräusel

Fraunhofer Institute for Machine Tools and Forming Technology IWU

Agnes Koschmider

University of Bayreuth

Martin Dix

Fraunhofer Institute for Machine Tools and Forming Technology IWU

Research Article

Keywords: forming, Shear cutting, Finite element analysis, Simulation, Machine learning, Surrogate model

Posted Date: November 24th, 2026

DOI: https://doi.org/10.21203/rs.3.rs-10691953/v1

License: This work is licensed under a Creative Commons Attribution 4.0 International License.
Read Full License

Additional Declarations: No competing interests reported.

A Data-Driven Surrogate Model for Tool Design Optimization in Multi-Stage Shear Cutting and Collar Forming Processes

Daniel L. Hahn[1*], Frederik Fonger[2], Patrik T. Michalski[3], Matthias Riemer[1], Verena Kräusel[1], Agnes Koschmider[2], Martin Dix[1]

[1]Fraunhofer Institute for Machine Tools and Forming Technology IWU, Reichenhainer Strasse 88, Chemnitz, 09126, Germany.
[2]University of Bayreuth, Wittelsbacherring 8, Bayreuth, 95444, Germany.
[3]Kiel University, Christian-Albrechts-Platz 4, Kiel, 24118, Germany.

*Corresponding author(s). E-mail(s): daniel.luca.hahn@iwu.fraunhofer.de;
Contributing authors: frederik.fonger@uni-bayreuth.de; ptm@informatik.uni-kiel.de;
matthias.riemer@iwu.fraunhofer.de; verena.kräusel@iwu.fraunhofer.de;
agnes.koschmider@uni-bayreuth.de;

Abstract

In multi-stage sheet metal forming processes such as combined shear cutting and collar forming, edge cracking is a relevant concern for process reliability. Predicting the influence of material and tool design parameters using finite element analysis (FEA) is computationally expensive, restricting its use in iterative design and optimization. This study therefore proposes a surrogate modeling and optimization workflow based on a scalar data representation for the shear cutting and collar forming process. A multilayer perceptron (MLP) is trained on a dataset of 2D simulations conducted in LS-DYNA to predict the circumferential strain at the collar edge, which serves as a strain-based indicator for comparing process configurations. The surrogate model is combined with the L-BFGS-B optimization algorithm to identify configurations that minimize the circumferential strain. The surrogate-assisted configuration is then evaluated using additional FEA simulations. Shapley values are used to quantify the contributions of the input parameters and assess their consistency with established process knowledge. The results demonstrate the potential of the proposed workflow for computationally efficient surrogate-assisted tool design. The Chebyshev-based parametrization offers a unified description for different collar punch geometries, enabling their reconstruction and integration into the workflow. Nevertheless, the findings are limited by the investigated design space and the predictive capabilities of the surrogate model.

Keywords: Collar forming, Shear cutting, Finite element analysis, Simulation, Machine learning, Surrogate model

1 Introduction

Collar forming, also known as hole flanging, is widely used in sheet metal forming processes to produce functional design elements for stiffening, spacing, fixing, and joining components [1]. During collar forming, a pre-hole, typically created by shear cutting (Fig. 1a), is expanded by a larger punch to form a continuous raised collar (Fig. 1b)

around the hole [2]. Edge cracking is an important process limitation and typically occurs at the outer edge of the collar where the maximum tangential tensile stresses σ_t are concentrated. The geometric expansion during collar forming can be characterized by the expansion ratio $a = d_1/d_0$ [1]. The limiting hole expansion ratio (HER), as defined in ISO 16630, additionally considers the onset of through-thickness cracking and therefore represents a measure of edge formability [3]. The achievable expansion ratio depends on material properties and punch geometry but is primarily influenced by the quality of the sheared edge and the diameter of the pre-hole d_0 [4].

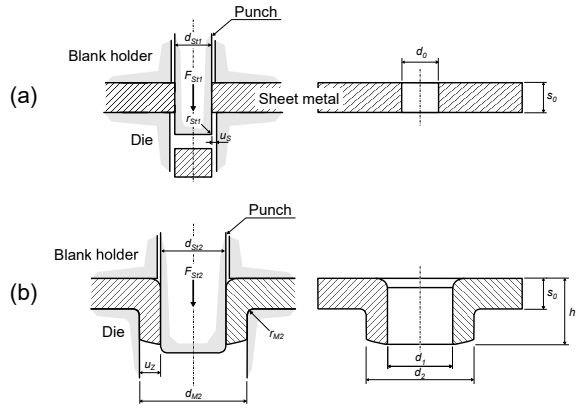

Fig. 1 Schematic of **a** shear cutting for pre-hole manufacturing and **b** collar forming process in reference to [5].

The sheared edge stretchability of advanced high-strength steels has been extensively investigated, with particular relevance to their increasing use in automotive applications [6]. Deformation within the shear-affected zone and heterogeneities along the sheared edge can reduce formability and promote early crack initiation during subsequent forming operations [7]. Complementary data-driven approaches have been developed to predict the HER based on material properties, process parameters, and sheared edge quality [8]. Recent experimental studies further highlight the strong influence of tool design parameters on edge crack formation [9].

In addition, Finite Element Analysis (FEA) enables the assessment of the shear cutting and collar forming process under varying tool parameters [1]. These simulations provide insight into the influence of the cutting clearance (u_S) during punching, as well as the drawing clearance (u_Z), die radius (r_{M2}) and punch geometry on the stress and strain distributions. For example, Thipprakmas et al. [10] demonstrated that fine blanking improved formability and reduced the appearance of edge cracks compared to conventional punching. FEA was also employed by Thipprakmas and Phanitwong [5] to investigate the influence of collar forming direction relative to burr orientation, while Sartkulvanich et al. [11] examined the influence of different punch geometries on the HER. Sandin et al. [7] combined Particle Finite Element Method-based shear cutting simulations with 3D hole expansion simulations and experiments, showing that circumferential heterogeneities reduce formability more strongly than through-thickness deformation within the shear-affected zone. However, model complexity directly influences the computational resources needed. For example, the detailed 3D simulation for shear cutting and hole expansion developed in [12] requires approximately 16 hours using eight CPU cores. Consequently, evaluating multiple tool or part design variants through FEA alone can be computationally expensive, motivating the use of surrogate models for industrial application [13].

Surrogate models approximate the relationship between input (part and tool design parameters) and output variables (simulation result). The specific output variable is defined by the underlying optimization problem. Jakumeit et al. [14] categorize these in: (1) a final component free of defects, (2) a final component free of wrinkles, (3) a final component meeting the desired geometric shape, and (4) the springback effect. In [13] and [15], surrogate models were developed to predict springback in a two-stage sheet metal forming process involving deep drawing and trimming. Zhou et al. [16] applied surrogate models to estimate the maximum equivalent plastic strain during deep drawing simulations.

Surrogate models typically employ machine learning (ML) techniques, ranging from classical regression methods to Artificial Neural Networks, to learn patterns from simulated datasets [17]. The selection of the modeling technique is also influenced by data representation used to describe the input and output parameters. Zhou et al. [16] distinguish between scalar and image

based methods. Scalar-based methods rely on low-order data representations, in which geometries are parameterized using simple approximations such as radii, angles, and lengths [13]. This representation enables the use of structured tabular inputs for regression-based models or feedforward neural networks, such as multilayer Perceptrons. However, this simplification limits the model's ability to generalize and transfer to more complex geometries.

Image-based ML approaches represent design parameters and simulation outputs as images, enabling spatially resolved learning [15]. For example, Convolutional Neural Networks (CNN) can map image-based design inputs directly to full-field strain distributions, preserving spatial information to improve accuracy and generalization [16]. Multi-view Convolutional Neural Network (MVCNN) architectures have also been applied to springback prediction by representing 3D FEA data as stacked depth images [13].

Higher-order data representations use 3D point clouds or graphs directly derived from the FEA results and meshes [13]. Heinzelmann et al. [15] employed a Graph Convolutional Network (GCN) for springback prediction in deep drawing simulations. In [13], springback prediction was performed using PointNet++ and Dynamic Graph Convolutional Neural Networks (DGCN) trained on point cloud data, achieving performance comparable to that of a MVCNN based on image representations. Despite their ability to capture complex geometric information, these approaches can require substantial computational resources and complex model architectures. In contrast, scalar-based representations offer a more efficient and interpretable alternative, particularly when the underlying geometry can be described using a limited set of physically meaningful features. An overview of the discussed approaches is provided in Table 1.

Therefore, this study proposes a surrogate modeling and optimization workflow for the two-stage shear cutting and collar forming process using a scalar-based representation of material and tool design parameters. The circumferential strain at the collar edge is predicted using a multilayer perceptron (MLP) trained on data from 2D FEA simulations conducted in LS-DYNA. The circumferential strain serves as a comparative indicator of local edge deformation, which is relevant to edge-cracking susceptibility, but is not intended as a direct failure criterion or to predict crack initiation and fracture. To incorporate different collar punch geometries into the scalar representation, the 2D punch contour is parametrized using an eighth degree Chebyshev polynomial. Shapley values are used to explain the MLP predictions and assess their consistency with established process knowledge. Furthermore, the trained surrogate model is coupled with the gradient based L-BFGS-B optimization algorithm to identify promising parameter configurations that minimize the predicted circumferential strain within the investigated design space. The selected configuration, including the reconstructed collar punch geometry, is subsequently evaluated using an additional FEA simulation.

2 Methods

This section presents the methodology, from FEA-based data acquisition to surrogate model development and optimization. An overview of the workflow is provided in Fig. 2.

2.1 Numerical simulation for shear cutting and collar forming

The numerical simulation setup of the combined shear cutting and collar forming process considers a critical configuration defined by a pre-hole diameter (d_0) of 6 mm and an inner collar diameter (d_1) of 13 mm, corresponding to an expansion ratio of $a = 2.17$. Both processes were modeled in LS-DYNA using an explicit time integration method. As shown in Fig. 3, the models consist of a punch, a blank holder, and a die, all of which are modeled as rigid bodies, in line with common practice reported by Thipprakmas and Phanitwong [5] and Basak et al. [18]. A 2D axisymmetric solid element formulation with volume weighting (ELFORM = 15) was employed to represent the rotational symmetry about the y-axis. The tool meshes were generated using the ANSA pre-processor, with a surface element size of 0.01 mm. Contact between the blank and the tooling was modeled using three automatic surface-to-surface mortar contact interfaces, covering the blank–support, upper wedge, and blank–tool interactions. A static friction coefficient of 0.20 was applied to all interfaces during shear cutting.

Table 1 Comparison of surrogate-model approaches for sheet-metal forming processes. The data set size refers to the number of unique simulation runs reported by the authors.

Reference	Input	Data set	ML model	Output	Validation strategy
Zhou et al. [16]	Image- and scalar-based	1,080	Res-SE-U-Net, MLP	Equivalent plastic strain (field/maximum)	Train/test split; unseen-geometry tests (extrapolation)
Heinzelmann et al. [15]	Graph-based	433,026	GCN	Springback vector field	Train/val/test split
Baum et al. [13]	Image- and point-cloud-based	160	MVCNN, PointNet++, DGCNN	Springback angles	Train/val/test split; model benchmark
This study	Scalar-based	5,400	MLP	Circumferential strain	Train/val/test split; additional FEA verification

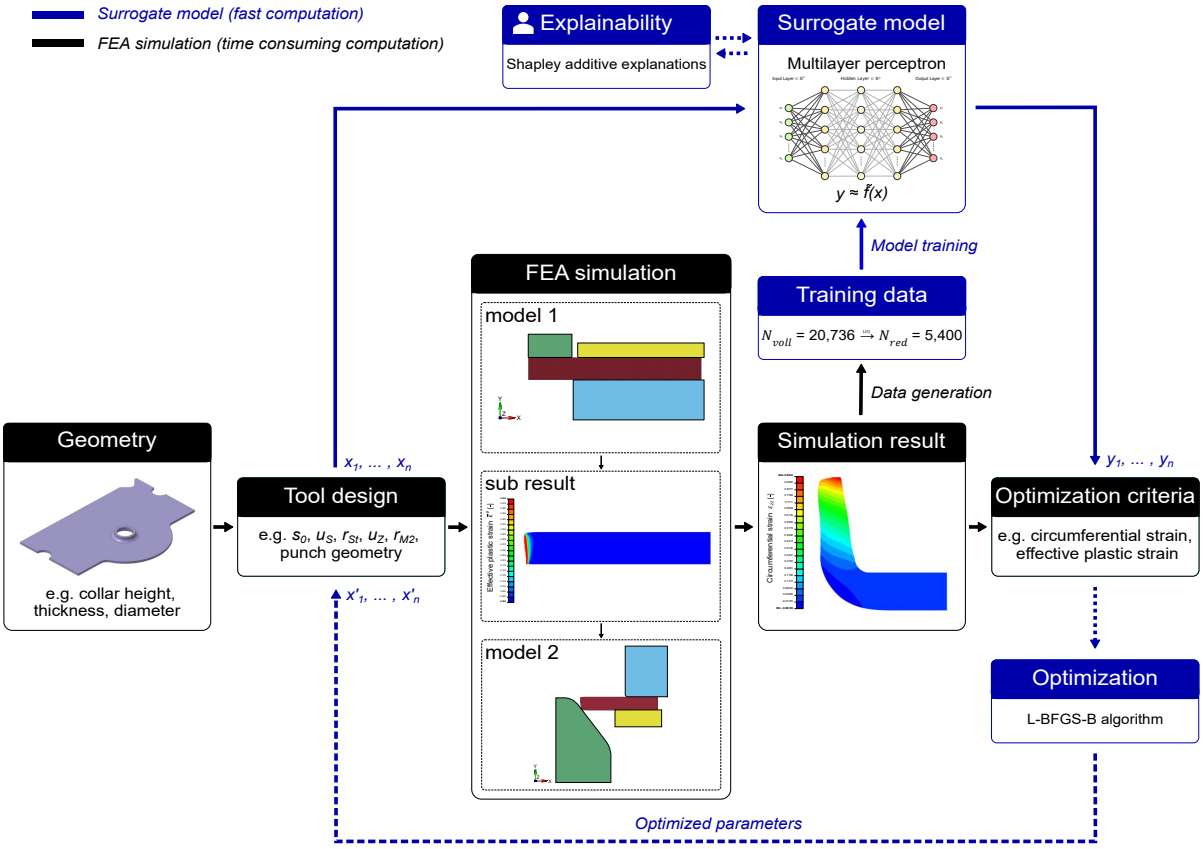

Fig. 2 Schematic visualization of the surrogate model pipeline

The material behavior of the investigated high-strength low-alloy steel S500MC was modeled using the elasto-plastic MAT_024 model (*MAT_PIECEWISE_LINEAR_PLASTICITY). Tensile tests were conducted in 0°, 45°, and 90° orientations relative to the rolling direction using a Zwick universal testing machine Z100 in accordance with ISO 6892-1 [19]. The resulting flow curve, used as input for the MAT_024 model, was approximated using the Hockett–Sherby exponential hardening approach [20]. Although tensile tests were conducted in three orientations,

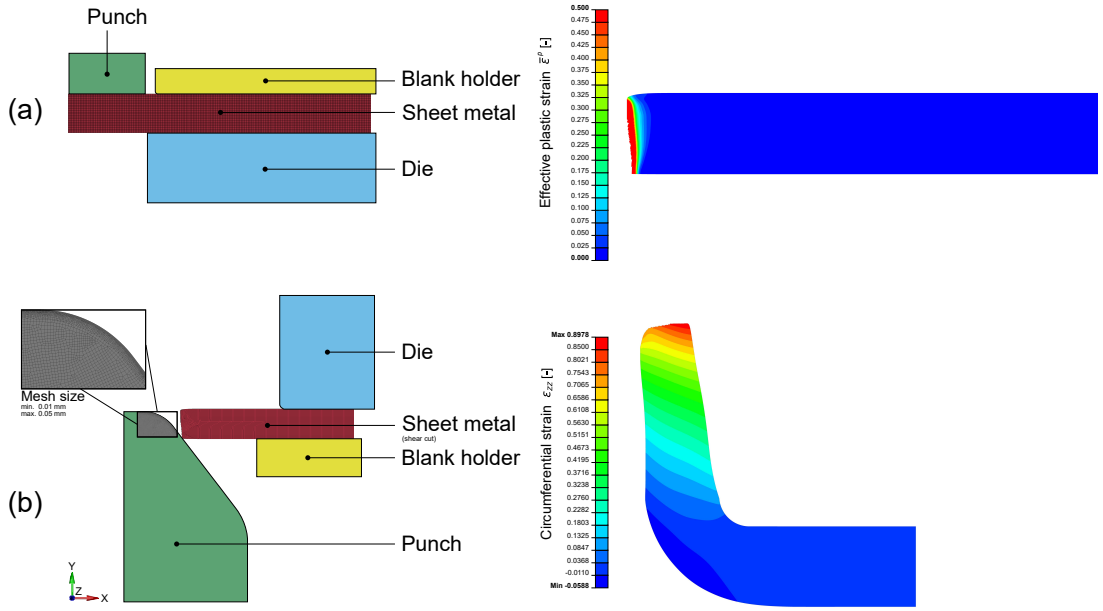

Fig. 3 Simulation setup and result for **a** shear cutting and **b** collar forming operation

MAT_024 assumes isotropic plasticity and does not capture directional material behavior. This simplification was adopted to maintain a manageable material description while focusing on the overall simulation and optimization workflow. Material failure behavior during shear cutting was modeled using the Generalized Incremental Stress State Dependent Damage Model (GISSMO) [21]. The corresponding GISSMO parameters were determined from additional material characterization tests using small tensile specimens (uniaxial tension), notched tensile specimens (elevated stress triaxiality), and shear tensile specimens loaded at 0° and 45° (shear-dominated and mixed loading conditions), following the recommendations of Andrade et al. [21]. Parameter calibration was performed in LS-OPT through inverse modeling, following the process flow presented by Galiev et al. [22]. The instability and failure strain curves were adjusted to achieve agreement between simulated and experimental force–displacement curves across the investigated stress states. All characterization tests were conducted under quasi-static loading conditions at room temperature. Strain rate- and temperature-dependent failure effects were not considered. No element-size regularization was applied to GISSMO, and the failure behavior may therefore remain dependent on the mesh size. Based on the mesh study presented in Appendix A, an element size of $h = 0.025$ mm was selected for the blank. For the evaluated $\varepsilon_{zz,3}$, this resolution results in a relative difference of 0.33% compared with the finest investigated mesh ($h = 0.015$ mm), while reducing the total computational time by approximately 74%.

The shear cutting process (Fig 3a) was modeled under displacement control by prescribing the punch movement in the negative y-direction through *BOUNDARY_PRESCRIBED_MOTION_RIGID and a corresponding loading curve. Material separation during shear cutting was modeled using the GISSMO in combination with element erosion. Element deletion is triggered upon reaching a critical damage value, thereby allowing material separation during shear cutting to be represented through damage accumulation and element erosion. To maintain mesh quality under the severe local deformations occurring in the cutting zone, adaptive re-meshing was employed throughout the simulation. Upon completion, the shear-cut blank, including its resulting geometry and relevant history-dependent state variables such as stresses and strains, was exported using the dynain functionality. These quantities were subsequently transferred to the collar forming simulation to account for the deformation and

stress state induced by the preceding shear cutting operation. The GISSMO damage variables were not transferred to the subsequent simulation.

For the subsequent collar forming simulation (Fig. 3b), punch motion was prescribed using a smooth loading curve. No additional damage or fracture model was applied. Finally, the dynain functionality was used to export the simulation results for subsequent analysis and processing.

The numerical results were validated by comparing the simulated force–displacement curves and final geometries with experimental data available in [23]. Samples with a sheet thickness s_0 of 1.6 mm were punched and formed using a ZS650CN hydraulic press manufactured by Schütz+Licht. For each parameter variation, five samples were manufactured. Further details regarding tooling and process parameters are provided in [9]. As shown in Fig 4, the simulated force–displacement curves and resulting geometries show good agreement with the experimental data. The geometric comparison shown in Fig. 4c is based on one representative sample, outlined in red, that was selected for optical measurement. Deviations between experiment and simulation may be partly attributed to the anisotropic material behavior, which is not captured by the isotropic MAT_024 formulation, as well as to deviations between the idealized tooling geometry and the actual manufactured tools. An anisotropic material model, such as Barlat YLD2000 (MAT_133) will therefore be considered for future investigations. The simulated force response during shear cutting (Fig. 4a) exhibits a steeper increase due to the rigid tool assumption, whereas the experimental curves reflect the elasticity of the tooling. To account for this behavior, mechanical springs can be incorporated into the model, as demonstrated in [24]. Good agreement between simulation and experiment was achieved for the maximum cutting force $F_{\max}$, the collar-forming force-displacement response (Fig. 4b), and the final geometry (Fig. 4c). Therefore, the rigid tool formulation was retained for the subsequent data acquisition presented in Section 2.2.

2.2 Data acquisition

For data acquisition, a design of experiments (DoE) was defined by systematically varying material and tool design parameters of both process stages (Fig. 1). As the shear cutting simulation was substantially more computationally demanding than the collar forming simulation, requiring approximately 2.19 hours on 40 CPU cores per simulation, only 54 shear cutting variants were generated. These variants were obtained by varying the cutting clearance u_{S}, sheet thickness s_0, punch cutting edge radius r_{St1}, and material behavior, as shown in Table 2. Variations in material behavior were introduced by scaling the flow curve to represent different levels of flow stress. For the collar forming simulation, the drawing clearance u_{Z}, die radius r_{M2}, and friction coefficient R were varied to represent different lubrication conditions (Table 2). As shown in Fig. 5, six different punch geometries (Geo_{St2}) were considered.

Table 2 Variations of material and tool design parameters

Parameter	Unit	Variation
Shear cutting		
Cutting edge radius r_{St1}	mm	{0.01, 0.1}
Cutting clearance u_{S}	mm	{0.1, 0.15, 0.2}
Sheet thickness s_0	mm	{1.55, 1.6, 1.65}
Flow curve scaling c_{f}	%	{94, 100, 106}
Collar forming		
Punch geometry Geo_{St2}	–	{KON60°, KON75°, PAR, HEM, RAD10, RAD30}
Friction coefficient R	–	{0.15, 0.2, 0.25, 0.3}
Drawing clearance u_{Z}	mm	{1.3, 1.5, 1.6, 1.7}
Die radius r_{M2}	mm	{0.3, 0.7, 1.0, 1.5}
Sheet thickness s_0	mm	{1.55, 1.6, 1.65}
Flow curve scaling c_{f}	%	{94, 100, 106}
Shear cutting variant	–	{1,. . . ,54}

The 54 shear cutting variants, combined with all parameter combinations of the collar forming simulation, would result in a total of 20,736 simulation runs for a full-factorial design. Therefore, randomized Latin hypercube sampling (LHS) was employed to reduce the number of collar forming simulations per shear cutting variant to 100, resulting in a total of 5,400 simulation runs. This approach provides a compromise between computational cost and sampling quality, reducing the total number of simulations by approximately

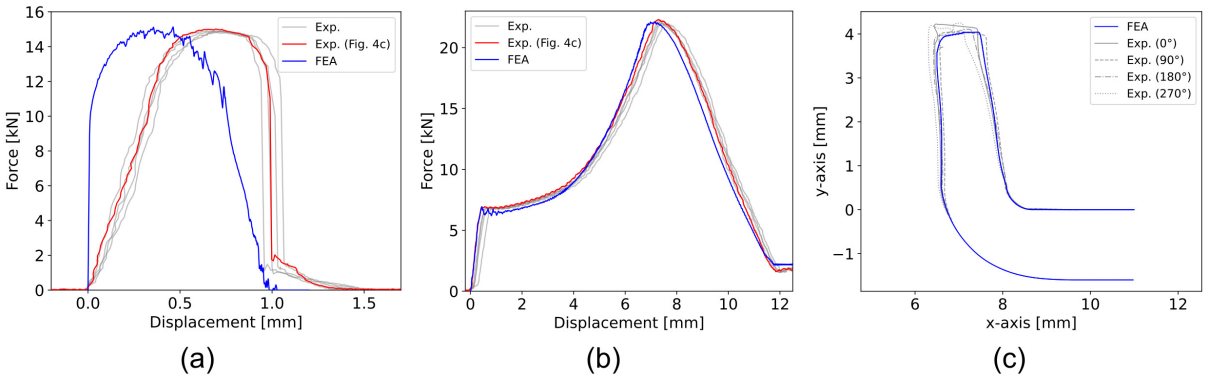

Fig. 4 Comparison of the force-displacement curves obtained from simulation and experiment for (**a**) the shear cutting process, (**b**) the collar forming process, and (**c**) the final geometry of the optically measured sample outlined in red.

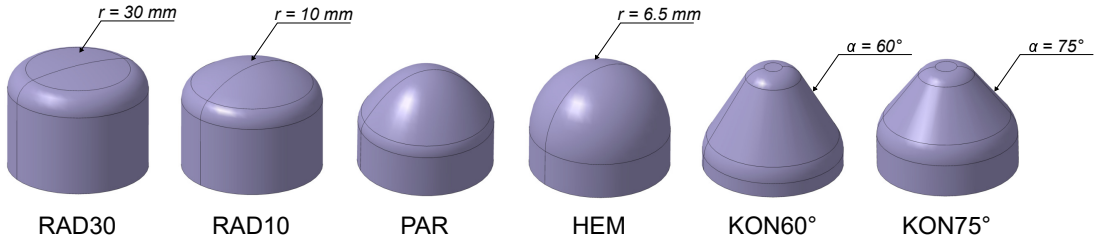

Fig. 5 Reference punch geometries considered in the collar forming process

74% while providing coverage of the design space for surrogate model training [25]. All simulation results, including the corresponding dynain and binout files, are made available through the dataset presented in [26].

The circumferential strain ε_{zz} at the upper collar edge was selected as the target variable to quantify the local deformation after the collar forming. To reduce sensitivity to local strain fluctuations, the collar edge was divided into three sectors. The mean circumferential strain was calculated for each sector, yielding $\varepsilon_{zz,1}$, $\varepsilon_{zz,2}$, and $\varepsilon_{zz,3}$. The circumferential strain reflects the tangential stretching of the pre-hole during collar forming but does not constitute a direct failure criterion. Crack initiation also depends on the local stress state, material behavior, and the condition of the sheared edge resulting from the preceding cutting operation [7].

2.3 Scalar representation of the tool geometry

As shown in Fig. 1, the key design parameters of the shear cutting and collar forming operations (r_{St1}, u_S, r_{M2} and u_Z) can be directly represented as scalar quantities. In contrast, the punch geometry requires a dedicated parameterization approach, for which Chebyshev polynomials were adopted. This approach provides a practical and unified representation of different punch geometries through a common parameter set. Furthermore, it enables the reconstruction of optimized geometries and their direct transfer into computer-aided design (CAD) applications.

Chebyshev polynomials were chosen for their efficiency and numerical stability as a basis for approximating smooth curves. They are a family of orthogonal polynomials that can be used to approximate a given curve by a linear combination of basis functions [27]. A function $y(x)$ can be

represented as

$$y(x) = \sum_{k=0}^{n} c_k T_k(x), \tag{1}$$

where $T_k(x)$ denotes the k-th Chebyshev polynomial, c_k are the corresponding coefficients, and n is the polynomial degree. The Chebyshev polynomials can be defined recursively as

$$T_{k+1}(x) = 2x\,T_k(x) - T_{k-1}(x). \tag{2}$$

Taking advantage of the rotational symmetry, the 2D punch contours were imported directly from CAD as DXF files. The contours were subsequently sampled, and a Chebyshev polynomial was fitted over the domain $0 \leq x \leq 6.5$ mm, excluding the vertical side of the punch as seen in Fig. 6. The coefficients were determined by a least-squares approximation using the `Chebyshev.fit()` implementation provided by the NumPy library. Since Chebyshev polynomials provide a continuous description of the punch geometry, the local curvature can be evaluated from their derivatives as

$$\kappa(x) = \frac{|y''(x)|}{\left(1 + (y'(x))^2\right)^{3/2}}, \tag{3}$$

where $y'(x)$ and $y''(x)$ denote the first and second derivatives of the Chebyshev polynomial [28]. This enables a quantitative assessment of local geometric features for manufacturability. The polynomial degree was selected based on the root mean squared error (RMSE) between the fitted contour and the sampled data points

$$\mathrm{RMSE} = \sqrt{\frac{1}{N}\sum_{i=1}^{N}(y_i - \hat{y}_i)^2}. \tag{4}$$

An eighth degree Chebyshev polynomial provided a compromise between approximation accuracy and the number of model features. Across all six reference geometries, a mean RMSE of 0.031 mm was achieved. The resulting nine coefficients c_k $(k = 0, \ldots, 8)$ were extracted for each punch geometry and used as its scalar representation.

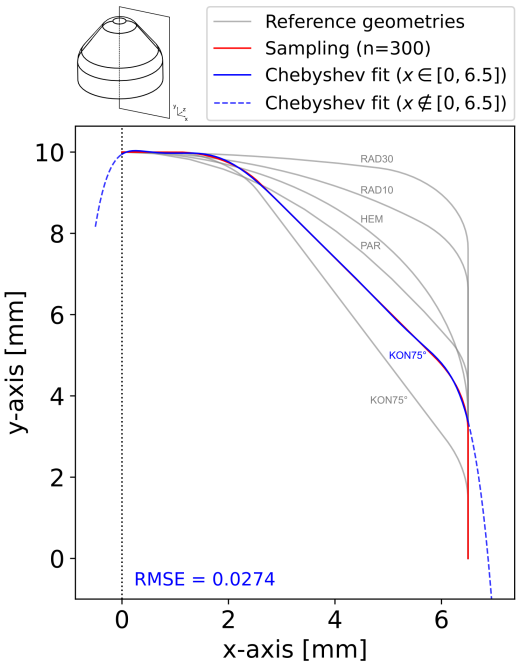

Fig. 6 2D parameterization of the geometry based on an eighth degree Chebyshev polynomial approximation for the 75° conical punch.

2.4 Machine learning model and training

The mean circumferential strain of the three sectors of the collar edge defined in Section 2.2 serves as the target variable. The MLP was selected for the mapping. MLPs are among the most widely used artificial neural networks for supervised learning of input–output relations and to approximate both linear and nonlinear functions [29]. For a scalar feature representation of moderate dimension, they require no assumptions about the structure of the input space.

The feature vector has sixteen entries. Seven of them are the material and tool design parameters of the shear cutting and collar forming operations, which are directly available as scalar quantities: sheet thickness s_0, flow curve scaling factor c_f, friction coefficient R, cutting edge radius r_{St1}, cutting clearance u_S, die radius r_{M2}, and drawing clearance u_Z. The remaining nine are the Chebyshev coefficients c_0 to c_8 of the punch contour introduced in Section 2.3. Material and tool design parameters are therefore combined in a single feature vector, with the punch geometry represented

by a set of continuous design variables for the optimization described in Section 3.3.

Inputs and targets were scaled before training, and the metrics reported in Section 3.1 refer to the scaled targets.

The model consists of an input layer with sixteen nodes, several hidden layers, and an output layer with three nodes, one for each sector of the upper collar edge. The architecture is shown in Fig. 7. Several configurations differing in the number and width of the hidden layers were trained and compared on the validation split. The lowest validation error was obtained with three hidden layers of 512, 512, and 256 nodes.

Of the dataset, 15% was withheld as a test set. The remaining data were split in a ratio of 85 to 15 into training and validation sets. The split was drawn at random across the individual simulations. The implications of this for the reported error are discussed in Section 3.1.

The trained surrogate model predicts the circumferential strain for a given combination of input parameters within a few milliseconds, which permits two applications. Combined with an optimization algorithm, it yields parameter combinations that minimize the strain at the collar edge, including the punch contour, which is the subject of Sections 2.5 and 3.3. As a stand-alone evaluation, it allows for the fast evaluation of parameter combinations.

2.5 SHAP-based explainability and L-BFGS-B optimization

Shapley values were used to relate the predictions of the surrogate model to the individual input features. Following the Shapley value of cooperative game theory, the method assigns each feature a contribution to the deviation of an individual prediction from the mean prediction of the model, and the contributions of all features sum to that deviation [30]. Evaluated across a dataset, the values yield both the relative importance of a feature and the direction of its influence on the output [31]. Shapley values were computed for all sixteen input features of the trained model on the samples of the test set, so that the explanation refers to data that were not used to fit the model. The results are discussed in Section 3.2.

The surrogate model was subsequently used as the objective function of a numerical optimization to determine the tool design parameters that minimize the circumferential strain at the collar edge. The design vector is the sixteen-entry feature vector of Section 2.4, so the seven material and tool design parameters and the nine Chebyshev coefficients of the punch contour are optimized jointly. Each variable is bounded: the parameters are limited to the ranges covered during data acquisition (Table 2) and the coefficients by the values that occur for the six sampled geometries. Since the trained network is differentiable with respect to its inputs, a gradient-based method can be applied. The L-BFGS-B algorithm was selected, a quasi-Newton method that approximates the inverse Hessian from a limited number of stored gradient differences and enforces simple bound constraints by gradient projection [32]. The limited-memory update keeps the cost per iteration low, and the bound handling restricts the search to the region in which the surrogate model fits. The optimization operates on the surrogate model alone. The resulting parameter set is verified by an FEA simulation of the reconstructed geometry, as described in Section 3.3.

3 Results and Discussion

The applicability of the proposed surrogate model for tool design is assessed from three perspectives: prediction accuracy, model explainability, and validation of the optimized punch geometry using FEA. Accordingly, Sections 3.1 to 3.3 evaluate the predictive performance of the model, analyze the learned input–output relationships, and demonstrate the closed-loop optimization workflow.

3.1 Prediction accuracy and generalization

The model was evaluated with the mean absolute error (MAE), the previously introduced RMSE according to Eq. 4, and the coefficient of determination R^2 [33, 34]. Table 3 lists the results on the validation and on the test set. On the test set R^2 reaches 0.989, so the residual variance amounts to approximately 1.1% of the variance of the target variable.

The MAE and RMSE are nearly identical for the validation and test sets, and the coefficients of determination differ by only 0.002. Since the validation set was used to select the network

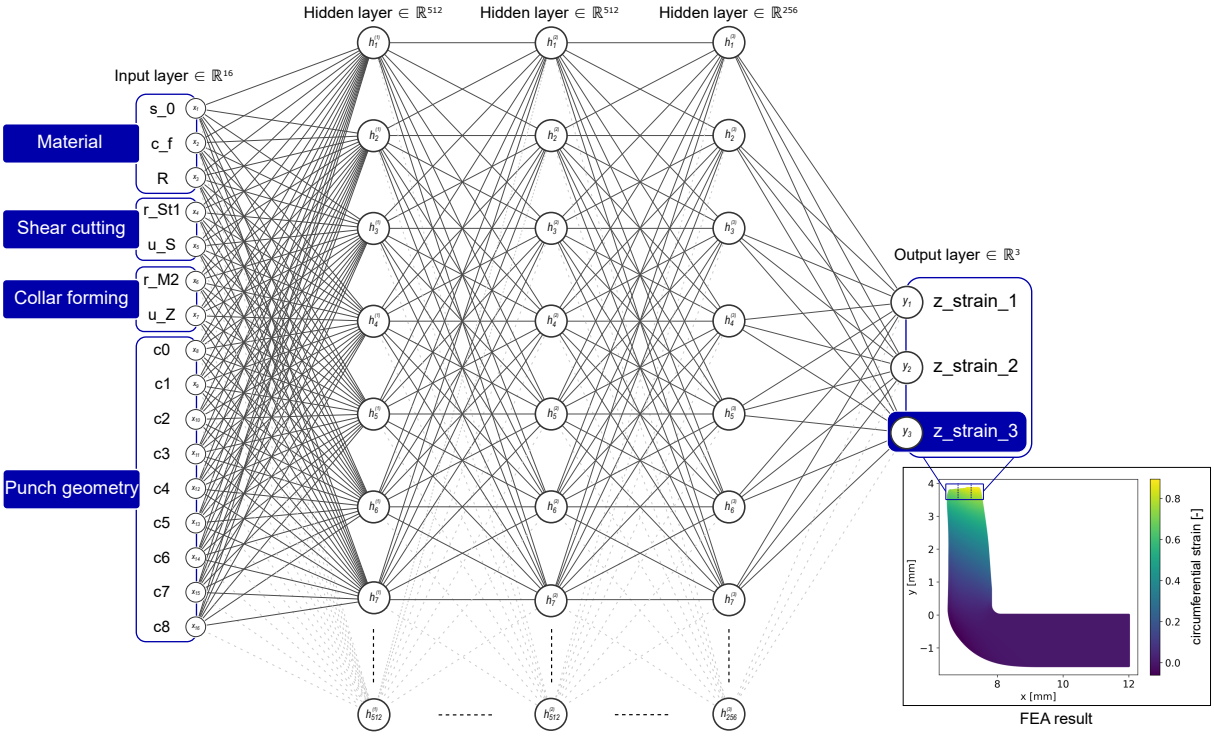

Fig. 7 Structure of the MLP neural network

architecture, this agreement indicates that the selected architecture performs similarly on both subsets. Within the sampled design space, the results therefore provide no indication of substantial overfitting.

The reported error quantifies interpolation within the sampled design space and is not a generalization estimate for new tool geometries. The 5,400 data points originate from 54 shear cutting states and six punch contours, so a randomly drawn split leaves neither a cutting variant nor a punch geometry unseen. Error estimates from splits that ignore such group structure are systematically optimistic [35]. Section 3.3 applies the model to precisely the case the split does not cover, a contour that has not been simulated. Withholding all samples of one punch contour at a time would quantify this transfer directly.

3.2 Explainable surrogate modeling

A low prediction error does not imply that a surrogate model has captured the mechanics of the process. It can also follow from regularities in the sampling design. Shapley values attribute each prediction to the individual input features, so the direction and the relative weight of the learned relationships can be compared with process knowledge [36]. Fig. 8 shows the values for all sixteen features, ordered by mean absolute contribution. The color encodes whether the feature value is high or low.

The four highest-ranked features are the sheet thickness s_0, the cutting clearance u_S, the cutting edge radius r_{St1}, and the friction coefficient R. An increase in s_0 raises the predicted strain, potentially reflecting the greater amount of material redistributed during collar forming. The three distinct SHAP clusters correspond to the discrete sheet thicknesses considered in the DoE (Table 2).

Table 3 Prediction performance of the MLP surrogate model on the validation and the test set, averaged over the three collar sectors.

Metric	Validation set	Test set
MAE	0.000453	0.000454
RMSE	0.00064	0.000643
R^2	0.991	0.989

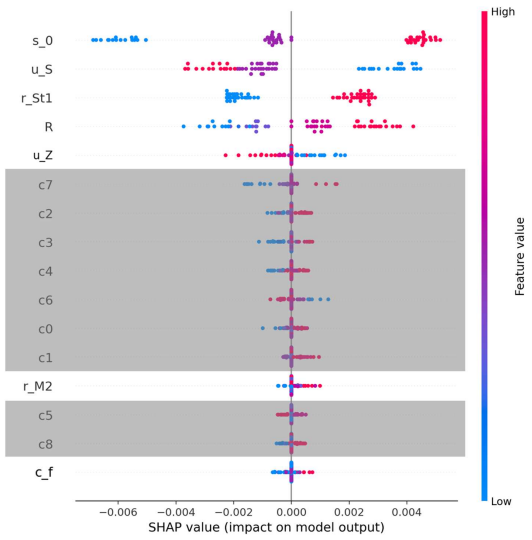

Fig. 8 Shapley values of the sixteen input features for $\varepsilon_{zz,3}$ at the collar edge. The nine Chebyshev coefficients of the punch contour are highlighted in gray.

A larger cutting clearance u_S is associated with a lower predicted ε_{zz} within the investigated range, potentially due to changes in the sheared edge geometry and the transferred stress and strain states from the preceding shear cutting operation. Experimental studies have reported different relationships between cutting clearance and edge formability, depending on the material and test method.

Feistle et al. [37] reported the maximum formability of the dual-phase steel at the highest investigated relative cutting clearance of 20%, using a self-developed edge-fracture-tensile test. In contrast, Frómeta et al. [38] identified an optimal relative cutting clearance of approximately 13–14% for dual-phase steel in their hole-tension tests, based on the strain at fracture. The decreasing $\varepsilon_{zz,3}$ observed in the present simulations should not be directly equated with the trends in edge formability and cracking susceptibility reported in these studies, as they are based on different test methods and evaluation criteria. Nevertheless, the largest relative cutting clearance investigated in the present simulations is 12.9%, extending the dataset to larger clearances would be useful to determine whether the decreasing strain trend continues or reverses at higher clearances.

A larger cutting edge radius r_{St1}, which can be associated with tool wear, increases the predicted ε_{zz}. This trend may reflect changes in the geometry and condition of the sheared edge generated during punching. Together, the contributions of u_S and r_{St1} indicate that the conditions established during shear cutting influence the subsequent strain response during collar forming.

However, the limited number of parameter variations currently restricts the interpretation of the SHAP results, particularly for the cutting edge radius r_{St1}, which was varied at only two levels. Furthermore, the smaller radius of 0.01 mm is below the blank element size of 0.025 mm, which limits its numerical resolution. Further investigations should therefore include intermediate cutting edge radii r_{St1}.

The friction coefficient R has a positive SHAP contribution, with higher values increasing the predicted ε_{zz}. This is consistent with reduced material flow under higher friction conditions, which promotes local stretching at the collar edge. The drawing clearance u_Z ranks fifth, with larger clearances reducing the predicted strain by facilitating material flow during collar forming. The die radius r_{M2} and the flow curve scaling factor c_f have comparatively little influence. This is plausible for r_{M2}, which primarily affects deformation in the region of the die radius rather than at the collar edge. The small contribution of c_f indicates that the investigated flow curve scaling of ±6% has a comparatively minor influence on the predicted strain.

None of the nine Chebyshev coefficients dominates the SHAP ranking. The five leading material and tool parameters rank above every coefficient c_k, while seven also rank above r_{M2} and all nine rank above c_f. However, this does not imply that the punch geometry has little influence, as the coefficients jointly represent a single design decision. They are strongly correlated because only specific combinations yield physically meaningful geometries, and the dataset contains only six distinct punch contours (Fig. 5). Since SHAP values computed under an assumption of feature independence can distribute the contribution of correlated features among individual coefficients [39], the individual attributions (Fig. 8) may understate the collective influence of the punch geometry. A comparison at the level of the design decision, the grouped attribution (the sum of the nine values per sample) is required.

3.3 Data-driven feedback loop for tool design optimization

The surrogate-based prediction was minimized over the bounded design space using the L-BFGS-B algorithm described in Section 2.5. The circumferential strain $\varepsilon_{zz,3}$ (z_strain_3) at the outer collar edge was used as optimization target, as this region exhibits the largest strains (Fig. 3). Table 4 lists the optimized parameter set. The Chebyshev coefficients c_0 to c_8 were used to reconstruct the punch geometry according to Section 2.3. As shown in Fig. 9a, the reconstructed geometry, which closely resembles an 80° conical punch, remains largely bounded by the reference geometries, except in the interval $0 < x < 1$ mm. This deviation can be attributed to the independent optimization of the Chebyshev coefficients, which combines characteristics of different reference geometries (Fig. 9b). Consequently, the contour was assessed in terms of its deviation from the reference geometries and its local curvature to evaluate its geometric feasibility and potential manufacturability. Using Eq. 3, a maximum curvature of $1.332\,\mathrm{mm}^{-1}$ was obtained, corresponding to a minimum radius of 0.751 mm. To reduce the sensitivity of point-wise curvature, a local mean curvature was additionally evaluated within a sliding window of 1 mm, yielding an effective radius of $r_{\mathrm{eff}} = 1.07\,\mathrm{mm}$. Although smaller than the 2 mm transition radii of the reference geometries, this value remains within a practically manufacturable range (Fig. 9). The reconstructed contour was then imported into CAD and adapted to the final geometry, outlined in red. Since this region remains outside the contact zone, the modification only simplifies mesh generation.

Evaluation was subsequently performed using the FEA model of Section 2.1, closing the loop between data acquisition, surrogate modeling, optimization, and verification without FEA evaluations during the search. Apart from the friction coefficient R, the optimized parameters lie at the boundaries of the investigated design space. Accordingly, the result is best described as a surrogate-assisted configuration, representing the minimum predicted $\varepsilon_{zz,3}$ within the prescribed parameter bounds, rather than an established optimum. This distinction is particularly important for the shear-cutting parameters, for which the DoE coverage remains limited and should therefore be extended in future investigations. For example, u_S lies at the upper boundary of the investigated range.

Table 4 Optimized material and tool design parameters obtained from L-BFGS-B

Parameter	Unit	Value
s_0	mm	1.55
c_f	%	94
R	–	0.180
r_{St1}	mm	0.010
u_S	mm	0.200
r_{M2}	mm	0.300
u_Z	mm	1.699
c_0	–	6.930
c_1	–	-2.725
c_2	–	-1.018
c_3	–	0.250
c_4	–	-0.190
c_5	–	-0.150
c_6	–	-0.030
c_7	–	-0.050
c_8	–	-0.060

To assess the local sensitivity of the surrogate-assisted configuration, an additional one-factor-at-a-time (OFAT) sensitivity analysis was conducted. The variations were evaluated using additional FEA simulations, with all remaining parameters kept at the surrogate-assisted configuration. Fig. 9c shows the resulting changes in $\Delta\varepsilon_{zz,3} = \varepsilon_{zz,3,\mathrm{var}} - \varepsilon_{zz,3,\mathrm{opt}}$, where positive values indicate an increase in $\varepsilon_{zz,3}$ compared with the surrogate-assisted configuration. The largest change was observed for s_0, with a maximum absolute deviation of approximately 0.0018. For comparison, across all 5,400 configurations $\varepsilon_{zz,3}$ spans a range of 0.0366, with a standard deviation of 0.00627 (Table B2). Thus, the largest change observed in the OFAT study amounts to approximately 5% of the overall strain range and 29% of its standard deviation. However, the maximum change observed in the OFAT analysis (0.00182) is smaller than the absolute strain difference of 0.00288 between the selected mesh size ($h = 0.025$ mm) and the finest investigated mesh ($h = 0.015$ mm), as reported in Appendix A. The comparison indicates that the individual OFAT effects cannot be conclusively established as mesh-independent. Furthermore, the OFAT analysis does not account for interactions between parameters or simultaneous variations and therefore cannot establish

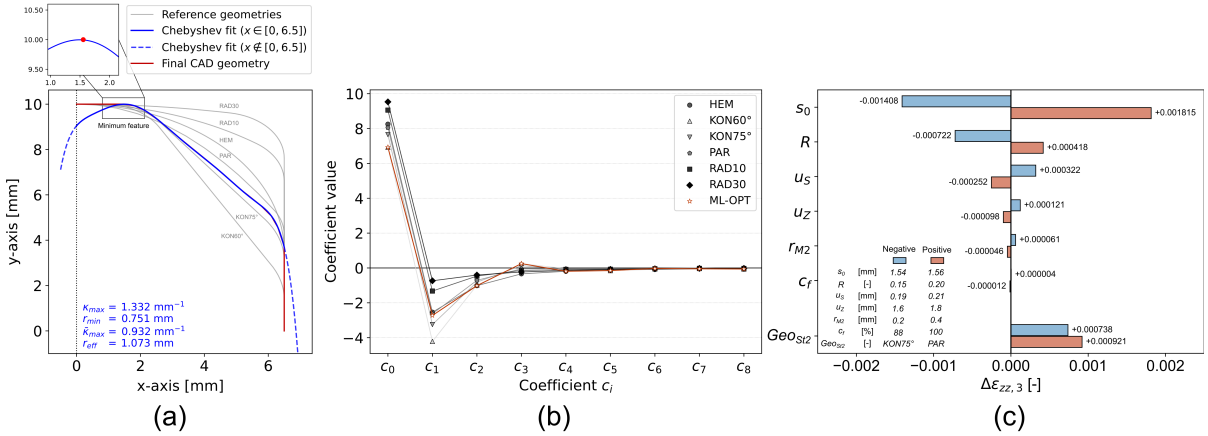

Fig. 9 Visualization of **a** the surrogate-assisted punch geometry, **b** the corresponding Chebyshev coefficients, and **c** the OFAT sensitivity analysis showing changes in $\Delta\varepsilon_{zz,3}$ relative to the surrogate-assisted configuration. Negative (blue) and positive (red) variations are shown separately. Parameters are ranked by their maximum absolute effect.

general robustness against manufacturing variability.

Since the surrogate-assisted punch contour lies mainly between the parabolic and the 75° conical reference geometries (Fig. 9), these two geometries were included as separate cases in the OFAT analysis. To further assess the influence of punch geometry, the surrogate-assisted configuration was subsequently compared with all six reference geometries (Fig. 5). Fig. 10 shows the resulting spatial distribution of the circumferential strain difference, defined as $\Delta\varepsilon_{zz} = \varepsilon_{zz,opt} - \varepsilon_{zz,ref}$. Negative values indicate a lower circumferential strain using the surrogate-assisted punch geometry. Since $\varepsilon_{zz,3}$ was defined as the optimization target (Fig. 7), the discussion focuses primarily on this region. Among the reference geometries, the largest reduction in circumferential strain is observed relative to the 10 mm and 30 mm radius punch geometries. At the burr side, a localized increase in $\Delta\varepsilon_{zz,3}$ can be observed, which is attributed to the deformation occurring during the initial contact with the punch.

The full-field strain distributions reveal that the reduction at the collar edge is accompanied by a redistribution of deformation within the collar wall. Compared to the conical and parabolic reference geometries, the surrogate-assisted contour generally reduces the circumferential strain at the collar edge while redistributing deformation within the collar wall. Lower values of ε_{zz} at the collar edge are obtained compared with the RAD10 and RAD30 geometries, whereas the reduction is only minor or negligible compared with the hemispherical punch.

The comparatively mixed improvement achieved by the surrogate-assisted geometry can be attributed to the Chebyshev representation, as discussed in Section 3.2. The L-BFGS-B algorithm treats the Chebyshev coefficients as independent variables, although only a limited set of physically meaningful coefficient combinations is represented by the six reference geometries. Consequently, the optimizer can explore regions of the feature space that are insufficiently represented in the training data. Despite the identified limitations, the proposed workflow demonstrates the feasibility of a closed-loop, data-driven framework combining surrogate modeling, explainability, optimization, and geometric reconstruction for tool design.

4 Conclusion

In this study, a data-driven surrogate modeling and optimization workflow for a two-stage shear cutting and collar forming process was developed. FEA simulations were used to model both operations, enabling the transfer of the deformed blank geometry and mechanical state variables, including stresses and strains, between the process stages. A dataset comprising 5,400 simulated variants was generated for surrogate modeling. Based on this, a MLP was trained to predict the circumferential strain ε_{zz} in three sectors at the collar edge. The collar punch geometry was parameterized using an eighth-degree Chebyshev

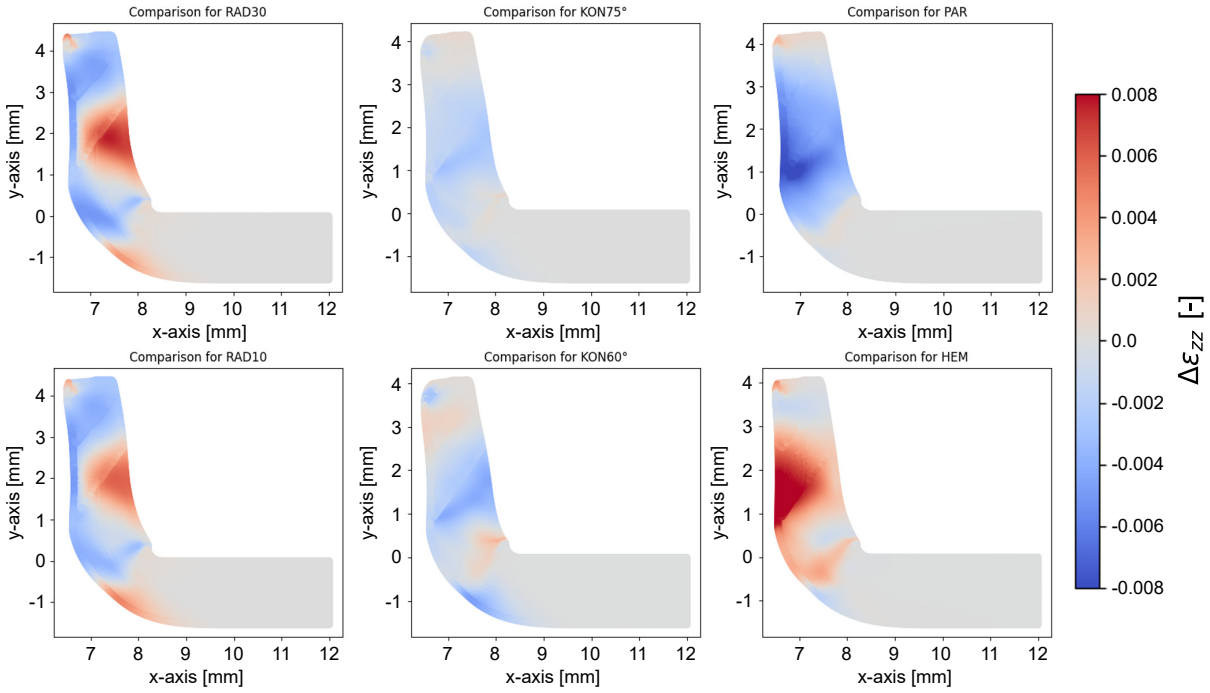

Fig. 10 Difference of the circumferential strain, $\Delta\varepsilon_{zz} = \varepsilon_{zz,\mathrm{opt}} - \varepsilon_{zz,\mathrm{ref}}$, between the surrogate-assisted punch and the six reference geometries, mapped onto the cross section of the formed part. Negative values (blue) indicate a lower ε_{zz} of the surrogate-assisted geometry.

polynomial, with its coefficients serving as scalar parameters. The MLP was subsequently combined with an L-BFGS-B optimization algorithm to identify material and tool design parameters that minimize the circumferential strain within the investigated design space. The resulting configuration was reconstructed geometrically and evaluated using additional FEA simulations.

SHAP analysis identified sheet thickness, cutting clearance, and cutting edge radius as the most influential parameters, while die radius and flow curve scaling factor had smaller contributions. Several of the identified relationships are qualitatively consistent with established process knowledge, providing an additional perspective on the model predictions. The small individual SHAP attributions of the nine Chebyshev coefficients reflect the distribution of a single geometric design across dependent features, rather than the unimportance of punch geometry.

Although the resulting geometry provides only mixed improvements relative to the reference geometries, it demonstrates the feasibility of a closed-loop strategy in which surrogate modeling, optimization algorithms, and CAD reconstruction are combined into a unified workflow. For the considered axisymmetric collar forming process, the combination of Chebyshev coefficients and physically meaningful scalar process parameters provides a compact and computationally efficient feature representation. An additional OFAT sensitivity analysis showed relatively limited changes in $\Delta\varepsilon_{zz,3}$ for the investigated parameter variations, with a maximum absolute change of approximately 0.0018. Although this change is smaller than the mesh-related difference of 0.00288 observed for the reference configuration, the numerical uncertainty of the relative parameter effects cannot be directly inferred from this comparison. Their mesh independence therefore remains unverified, and potential interactions between parameters were not investigated.

Two limitations restrict the transferability of the result. First, the optimization algorithm treats the Chebyshev coefficients as independent design variables, so the search may enter regions of the parameter space containing unrealistic or poorly

represented contours. Second, the reported prediction error was obtained from a randomly drawn split of a dataset that contains six punch contours and 54 cutting states, so it quantifies interpolation within the sampled design space rather than transfer to a contour that has not been simulated.

Future work will integrate geometric feasibility checks into the optimization workflow to ensure that reconstructed punch contours satisfy curvature and manufacturability constraints. Withholding one punch contour at a time from training will quantify the transfer between contour families. Finally, hybrid simulation-experimental datasets will be explored to reduce the simulation-reality gap and improve applicability to industrial tool design.

Acknowledgements. This work was funded by the Deutsche Forschungsgemeinschaft (DFG, German Research Foundation) in the SPP 2422 "Data-Driven Process Modeling in Forming Technology" [grant number 500936349]. The authors also want to thank Jakub Korenek for his work during the development of the numerical process simulation.

Data availability. The simulation dataset generated is publicly available in the Zenodo repository accessible under the URL: https://doi.org/10.5281/zenodo.18400421.

Declarations

Financial interest. The authors declare that they have no known competing financial interests or personal relationships that could have appeared to influence the work reported in this paper.

Competing interest. The authors declare no competing interests.

Appendix A Mesh study

A mesh study was conducted to determine a suitable element size for data acquisition (Section 2.2). The circumferential strain $\varepsilon_{zz,3}$ was selected for evaluating mesh dependency, as it represents the optimization target in Section 3.3. As shown in Table A1 and Fig. A1, mesh refinement leads to progressively smaller changes in $\varepsilon_{zz,3}$. For the selected element size of $h = 0.025$ mm, the absolute difference from the finest investigated mesh ($h = 0.015$ mm) is 0.00288, corresponding to a relative difference of 0.33%.

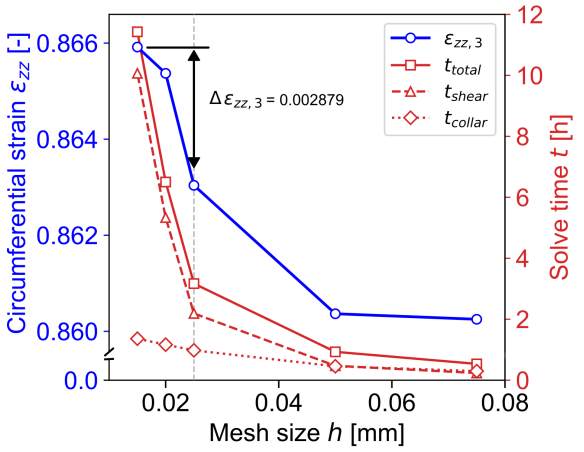

Fig. A1 Mesh study of $\varepsilon_{zz,3}$ and computational time for shear cutting t_{shear}, collar drawing t_{collar}, and the total simulation t_{total}.

Compared with the finest mesh, the selected resolution reduces the total computational time from 11.38 h to 2.99 h (approximately 74%). This represents a compromise between numerical accuracy and computational efficiency for the large-scale simulation campaign.

Appendix B Statistical Analysis of Circumferential Strain

The statistical distributions of the circumferential strain across the three collar-edge segments are summarized in Table B2 and illustrated using boxplots in Fig. B2. For each segment strain, the minimum, maximum, mean, and standard deviation are reported.

References

[1] Hoffmann, H., Neugebauer, R., Spur, G.: Handbuch Umformen, 1st edn. Edition Handbuch der Fertigungstechnik. Hanser, München (2012). https://doi.org/10.3139/9783446430044

Table A1 Mesh study results for $\varepsilon_{zz,3}$, including the number of elements N_{elements} and computational time for shear cutting t_{shear}, collar drawing t_{collar}, and the total simulation t_{total}.

h [mm]	N_{elements} [-]	$\varepsilon_{zz,3}$ [-]	t_{shear} [h]	t_{collar} [h]	t_{total} [h]
0.075	3,360	0.860251	0.24	0.51	0.74
0.050	7,680	0.860366	0.47	0.55	1.02
0.025	30,720	0.863039	2.19	0.80	2.99
0.020	48,000	0.865370	5.34	0.93	6.27
0.015	85,600	0.865918	10.07	1.31	11.38

Table B2 Minimum, maximum, mean and standard deviation of ε_{zz} across the three collar-edge segments for all 5,400 simulated process configurations.

Segment	$\varepsilon_{zz,1}$	$\varepsilon_{zz,2}$	$\varepsilon_{zz,3}$
Minimum	0.726167	0.808351	0.857867
Maximum	0.773375	0.837705	0.894492
Mean	0.746855	0.818199	0.870651
Standard deviation	0.009494	0.004408	0.006270

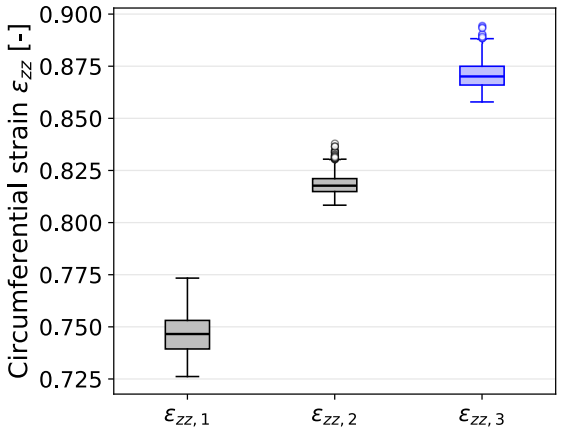

Fig. B2 Boxplots of ε_{zz} across the three collar-edge segments for all 5,400 simulated process configurations.

[2] DIN Deutsches Institut für Normung e.V.: DIN 8584-5: Manufacturing Processes — Forming Under Combined Tensile and Compressive Conditions — Part 5: Forming by Raising; Classification, Subdivision, Terms and Definitions. Standard, Berlin (2003)

[3] Paul, S.K.: A critical review on hole expansion ratio. Materialia **9**, 100566 (2020) https://doi.org/10.1016/j.mtla.2019.100566

[4] Lange, K. (ed.): Umformtechnik: Handbuch Für Industrie und Wissenschaft. Band 3: Blechbearbeitung, 2nd edn. Springer, Berlin, Heidelberg (1990). https://doi.org/10.1007/978-3-662-10686-0

[5] Thipprakmas, S., Phanitwong, W.: Finite element analysis of flange-forming direction in the hole flanging process. Int. J. Adv. Manuf. Technol. **61**(5), 609–620 (2012) https://doi.org/10.1007/s00170-011-3721-8

[6] Levy, B.S., Van Tyne, C.J.: Review of the shearing process for sheet steels and its effect on sheared-edge stretching. J. Mater. Eng. Perform. **21**(7), 1205–1213 (2012) https://doi.org/10.1007/s11665-011-9997-x

[7] Sandin, O., Larour, P., Hammarberg, S., Kajberg, J., Casellas, D.: The influence of cut edge heterogeneity in complex phase steel sheet edge cracking: An experimental and numerical investigation. Eng. Frac. Mech. **322**, 111176 (2025) https://doi.org/10.1016/j.engfracmech.2025.111176

[8] Jeong, K., Jeong, Y., Lee, J., Won, C., Yoon, J.: Prediction of hole expansion ratio for advanced high-strength steel with image feature analysis of sheared edge. Materials **16**(7), 2847 (2023) https://doi.org/10.3390/ma16072847

[9] Korenek, J., Riemer, M., Kräusel, V., Langhammer, D., Koschmider, A.: Experimental study on automation and data-driven modeling in the punching-collar forming process. at-Automatisierungstechnik **73**(3), 185–197 (2025) https://doi.org/10.1515/auto-2024-0104

[10] Thipprakmas, S., Jin, M., Murakawa, M.:

Study on flanged shapes in fineblanked-hole flanging process (fb-hole flanging process) using finite element method (fem). J. Mater. Process. Technol. **192–193**, 128–133 (2007) https://doi.org/10.1016/j.jmatprotec.2007.04.040

[11] Sartkulvanich, P., Kroenauer, B., Golle, R., Konieczny, A., Altan, T.: Finite element analysis of the effect of blanked edge quality upon stretch flanging of AHSS. CIRP Ann. **59**(1), 279–282 (2010) https://doi.org/10.1016/j.cirp.2010.03.108

[12] Qian, L., Ji, W., Sun, C., Fang, G., Lian, J.: Prediction of edge fracture during hole-flanging of advanced high-strength steel considering blanking pre-damage. Eng. Fract. Mech. **248**, 107721 (2021) https://doi.org/10.1016/j.engfracmech.2021.107721

[13] Baum, S., Heinzelmann, P., Liewald, M., Weyrich, M.: Enhancing fea sheet metal forming simulations through 3d geometric data-driven surrogate modeling. at-Automatisierungstech. **73**(4), 261–270 (2025) https://doi.org/10.1515/auto-2024-0116

[14] Jakumeit, J., Herdy, M., Nitsche, M.: Parameter optimization of the sheet metal forming process using an iterative parallel kriging algorithm. Struct. Multidiscip. Optim. **29**(6), 498–507 (2005) https://doi.org/10.1007/s00158-004-0455-3

[15] Heinzelmann, P., Baum, S., Riedmüller, K.R., Liewald, M., Weyrich, M.: A data-driven surrogate model for predicting spring-back in deep drawing processes. J. Phys.: Conf. Ser. **3104**(1), 012060 (2025) https://doi.org/10.1088/1742-6596/3104/1/012060

[16] Zhou, H., Xu, Q., Nie, Z., Li, N.: A study on using image-based machine learning methods to develop surrogate models of stamp forming simulations. J. Manuf. Sci. Eng. **144**(2), 021012 (2022) https://doi.org/10.1115/1.4051604

[17] Wang, H., Ye, F., Chen, L., Li, E.: Sheet metal forming optimization by using surrogate modeling techniques. Chin. J. Mech. Eng. **30**(1), 22–36 (2017) https://doi.org/10.3901/CJME.2016.1020.123

[18] Basak, S., Kim, C., Jeong, W., Jung, Y.I., Lee, M.-G.: Numerical prediction of sheared edge profiles in sheet metal trimming using ductile fracture modeling. Int. J. Mech. Sci. **219**, 107109 (2022) https://doi.org/10.1016/j.ijmecsci.2022.107109

[19] DIN Deutsches Institut für Normung e.V.: Metallic materials - Tensile testing - Part 1: Method of test at room temperature (ISO 6892-1:2019); German version EN ISO 6892-1:2019. Standard, Berlin (2020)

[20] Hockett, J.E., Sherby, O.D.: Large strain deformation of polycrystalline metals at low homologous temperatures. J. Mech. Phys. Solids **23**(2), 87–98 (1975) https://doi.org/10.1016/0022-5096(75)90018-6

[21] Andrade, F.X.C., Feucht, M., Haufe, A., Neukamm, F.: An incremental stress state dependent damage model for ductile failure prediction. Int. J. Fract. **200**(1), 127–150 (2016) https://doi.org/10.1007/s10704-016-0081-2

[22] Galiev, E., Linnemann, M., Winter, S., Psyk, V., Dix, M.: Determination of GISSMO damage parameters for high-speed blanking of 22mnb5 and en aw-5754. In: Proc. 10th Int. Conf. High Speed Form. (2025). https://doi.org/10.17877/DE290R-25688

[23] Korenek, J., Riemer, M., Kräusel, V., Hahn, D.L., Langhammer, D., Koschmider, A.: Experimental Study on Automation and Data-Driven Modeling in the Punching-Collar Forming Process [Dataset]. Zenodo (2026). https://doi.org/10.5281/zenodo.17866837

[24] Riemer, M., Silbermann, K., Kräusel, V., Langhammer, D., Koschmider, A.: Shear cutting: Model-based prediction of material parameters based on synthetic process force signals. In: Material Forming – ESAFORM 2024. Mater. Res. Proc., vol. 41, pp. 1334–1342. Mater. Res. Forum LLC, Millersville, PA (2024). https://doi.org/10.

21741/9781644903131-148

[25] Viana, F.A.C.: A tutorial on latin hypercube design of experiments. Qual. Reliab. Eng. Int. **32**(5), 1975–1985 (2016) https://doi.org/10.1002/qre.1924

[26] Korenek, J., Riemer, M., Hahn, D.L., Kräusel, V., Fonger, F., Michalski, P.T., Koschmider, A.: Data4Collar: Numerical Simulation Dataset for the Multi-Stage Shear Cutting and Collar Forming Process [Dataset]. Zenodo (2026). https://doi.org/10.5281/zenodo.18400421

[27] Mason, J.C., Handscomb, D.C.: Chebyshev Polynomials. Chapman & Hall/CRC, New York, NY, USA (2002). https://doi.org/10.1201/9781420036114

[28] Farin, G., Hoschek, J., Kim, M.-S. (eds.): Handbook of Computer Aided Geometric Design. Elsevier. https://doi.org/10.1016/B978-0-444-51104-1.X5000-X

[29] Taud, H., Mas, J.F.: Multilayer perceptron (MLP). In: Camacho Olmedo, M.T., Paegelow, M., Mas, J.-F., Escobar, F. (eds.) Geomatic Approaches for Modeling Land Change Scenarios, pp. 451–455. Springer, Cham (2018). https://doi.org/10.1007/978-3-319-60801-3_27

[30] Lundberg, S.M., Lee, S.-I.: A unified approach to interpreting model predictions. In: Advances in Neural Information Processing Systems, vol. 30, pp. 4765–4774. Curran Associates, Inc., Red Hook, NY, USA (2017)

[31] Marcilio, W.E., Eler, D.M.: From explanations to feature selection: Assessing SHAP values as feature selection mechanism. In: Proc. 33rd SIBGRAPI Conf. Graph., Patterns Images, pp. 340–347. IEEE, Recife/Porto de Galinhas, Brazil (2020). https://doi.org/10.1109/SIBGRAPI51738.2020.00053

[32] Byrd, R.H., Lu, P., Nocedal, J., Zhu, C.: A limited memory algorithm for bound constrained optimization. SIAM J. Sci. Comput. **16**(5), 1190–1208 (1995) https://doi.org/10.1137/0916069

[33] Rainio, O., Teuho, J., Klén, R.: Evaluation metrics and statistical tests for machine learning. Sci. Rep. **14**(1), 6086 (2024) https://doi.org/10.1038/s41598-024-56706-x

[34] Tatachar, A.V.: Comparative assessment of regression models based on model evaluation metrics. Int. Res. J. Eng. Technol. **8**(9), 853–860 (2021)

[35] Kapoor, S., Narayanan, A.: Leakage and the reproducibility crisis in machine-learning-based science. Patterns **4**(9), 100804 (2023) https://doi.org/10.1016/j.patter.2023.100804

[36] Liewald, M., Bergs, T., Groche, P., Behrens, B.-A., Briesenick, D., Müller, M., Niemietz, P., Kubik, C., Müller, F.: Perspectives on data-driven models and their potentials in metal forming and blanking technologies. Prod. Eng. **16**(5), 607–625 (2022) https://doi.org/10.1007/s11740-022-01115-0

[37] Feistle, M., Golle, R., Volk, W.: Determining the influence of shear cutting parameters on the edge cracking susceptibility of high-strength-steels using the edge-fracture-tensile-test. Procedia CIRP **41**, 1078–1083 (2016) https://doi.org/10.1016/j.procir.2016.01.007

[38] Frómeta, D., Lara, A., Parareda, S., Casellas, D.: Evaluation of edge formability in high strength sheets through a fracture mechanics approach. In: Proceedings of the 22nd International ESAFORM Conference on Material Forming (ESAFORM 2019), p. 160007 (2019). https://doi.org/10.1063/1.5112704

[39] Aas, K., Jullum, M., Løland, A.: Explaining individual predictions when features are dependent: More accurate approximations to Shapley values. Artif. Intell. **298**, 103502 (2021) https://doi.org/10.1016/j.artint.2021.103502